(22) Almog, Y.; Klein, J. *J. Colloid Interface Sci.* **1985**, *106*, 33.
(23) Hu, H.-W.; Van Alsten, J.; Granick, S. *Langmuir* **1989**, *5*, 270.
(24) Luesse, C.; Carson, G.; Van Alsten, J.; Granick, S. *Rev. Sci. Instrum.* **1988**, *59*, 811.
(25) Saeiki, S.; Kuwahara, N.; Konno, S.; Kaneko, M. *Macromolecules* **1973**, *6*, 589.
(26) Christenson, H. K.; Blom, C. E. *J. Chem. Phys.* **1987**, *86*, 419, and references therein.
(27) Christenson, H. K. *J. Chem. Phys.* **1983**, *78*, 6906. Horn, R. G.; Israelachvili, J. N. *J. Chem. Phys.* **1981**, *75*, 1400.
(28) Rossi, G.; Pincus, P. A. *Europhys. Lett.* **1988**, *5*, 641; *Macromolecules* **1989**, *22*, 276.
(29) It is true that the weak attraction in Figure 7 was not much larger than a conservative measure of the experimental uncertainty; if the experiments had been less stable, it might have been an artifact from a drift in the base line. However, it was reversible and reproducible in different experiments, so we report the data but do not rely upon it in the discussion.
(30) Mass adsorbed is sometimes gauged from the refractive index measured in hard contact. We attempted to do this, but unfortunately in our hands the measurements were too scattered to give a reliable estimate.
(31) Klein, J., personal communication.
(32) Kawaguchi, M.; Takahashi, A. *J. Polym. Sci., Polym. Phys. Ed.* **1980**, *18*, 2069.
(33) Freed, K. *Renormalization Group Theory of Polymers*; Wiley: New York, 1987; Chapters 8 and 10.
(34) In Figures 11 and 12, the unperturbed radii of gyration[44] were adjusted to account for expansion under better than Θ solvent conditions. The correction was estimated according to the two-parameter theory[33] as the factor $CM^{1/2}(T - T_\Theta)$. The system-specific constant, C, which in this instance describes polystyrene in cyclopentane, was fixed by comparison to the recent light-scattering experiments of Berry and co-workers.[21] The inflation of R_G from this calculation does not affect the conclusion. The largest correction was by a factor of 1.08 (polymer D at 34 °C).
(35) Israelachvili, J. N. *Intermolecular and Surface Forces*; Wiley: New York, 1985.
(36) Ploehn, H. J.; Russel, W. B. *Macromolecules* **1989**, *22*, 276.
(37) Klein, J.; Luckham, P. F. *Macromolecules* **1986**, *19*, 2007.
(38) Watanabe, H.; Patel, S.; Tirrell, M. *Polym. Prepr. (Am. Chem. Soc., Div. Polym. Chem.)* **1988**, *29*, 370; *ACS Symp. Ser.*, in press.
(39) Ingersent, K.; Klein, J.; Pincus, P., submitted for publication in *Macromolecules*.
(40) Scheutjens, J. M. H. M.; Fleer, G., private communication.
(41) Kremer, K. *J. Phys. (Les Ulis, Fr.)* **1986**, *47*, 1269.
(42) Van Alsten, J.; Granick, S. *Phys. Rev. Lett.* **1988**, *61*, 2570. Van Alsten, J.; Granick, S., unpublished experiments.
(43) Zapas, L. J.; McKenna, G. B.; Brenna, A. *J. Rheol.* **1989**, *33*, 69.
(44) Schmidt, M.; Burchard, W. *Macromolecules* **1981**, *14*, 210.
(45) Horn, R. G.; Israelachvili, J. N.; Pribac, F. *J. Colloid Interface Sci.* **1987**, *115*, 480.
(46) Israelachvili, J. N.; McGuiggan, P. M.; Homola, A. M. *Science* **1988**, *240*, 189.
(47) Muller, K.; Chang, C. C. *Surf. Sci.* **1969**, *14*, 39.
(48) Dowsett, M. G.; King, R. M.; Parker, E. H. C. *J. Vac. Sci. Technol.* **1977**, *14*, 771.
(49) Israelachvili, J. N.; Horn, R., private communication.
(50) Asthana, A. M.S. Thesis, University of Illinois at Urbana-Champaign, 1987.
(51) Horn, R. G.; Hirz, S. J.; Hadzzioannou, G.; Frank, C. W.; Catala, J. M. *J. Chem. Phys.* **1989**, *90*, 6767.
(52) Johnson, H. E.; Granick, S., unpublished results.

Registry No. PS, 9003-53-6.

Chain Length and the Cosolubility of *n*-Paraffins in the Solid State

Douglas L. Dorset

Electron Diffraction Department, Medical Foundation of Buffalo, Inc., Buffalo, New York 14203-1196. *Received May 11, 1989; Revised Manuscript Received June 23, 1989*

ABSTRACT: Within the constraints of rectangular layer chain packing and the orthorhombic perpendicular methylene subcell imposed by the crystal structure, a chain length series of *n*-paraffins from $C_{28}H_{58}$ to $C_{60}H_{122}$ was used to form binary solids. If chain length differences fall within limits similar to those found in earlier analyses, solid solutions are formed. As indicated by theoretical calculations of the melting point line, they are nearly ideal in their behavior. Outside of this chain length difference eutectics are formed, with liquidus curves also corresponding closely to the freezing point depression of an ideal liquid solution. Depending on chain length difference, the eutectic solid will be composed of an incommensurate layer structure (crystallized from a metastable solid solution) coexisting with the longer chain component. If no cosolubility is possible, a mixture of the two pure components separates. A boundary domain also exists before strict eutectic separation when a critical temperature is reached. Here, at the miscibility gap, metastable solid solutions fractionate, with a structure very similar to that of a secondary eutectic solid for binary combinations where limited solid solubility still exists. However, the incommensurate solid changes continuously with concentration unlike the mixed lamellar stacking in the eutectic, which has a constant composition. It is therefore possible to describe a progression of crystalline arrays between the stable solid solution and fully separated eutectic.

Introduction

n-Paraffin binary solids have received considerable attention for many years[1-16] as models for the polydisperse polymethylene chain packings found in polyethylene lamellae as well as the mixed acyl chain layers in biomembrane lipids. From numerous calorimetric and diffraction studies, a number of factors can be envisioned that could affect the solid solubility of two paraffins, including the space groups of the pure components as well as their relative chain lengths (i.e., respective molecular volumes), as stated formally by Kitaigorodskii.[17]

Recently[18,19] we have found that the symmetry rules thought to govern the stability of an *n*-paraffin solid are somewhat restrictive, and indeed, within a series of solid solutions composed of paraffins that crystallize in the same space group, there is no continuity of space group symmetry, but only a continuum of methylene subcell

0024-9297/90/2223-0623$02.50/0

Table I
Orthorhombic *n*-Paraffins Used for the Formation of Binary Solids

compound	source	purity	T^m(obs), °C	T^m(calc), °C	ΔH(obs), J/g	ΔH(calc), J/g
n-octacosane ($C_{28}H_{58}$)	*e*	97%	62.9	59.7	212.7	262.2
n-triacontane ($C_{30}H_{62}$)	*a*	99%	65.8	64.2	235.4	264.3
n-dotriacontane ($C_{32}H_{66}$)	*b*	>95%	69.6	68.4	233.4	266.1
n-tritriacontane ($C_{33}H_{68}$)	*c*	>97%	71.2	70.3	234.6	254.5
n-tetratriacontane ($C_{34}H_{70}$)	*a*	99%	72.9	72.1	230.0	267.8
n-pentatriacontane ($C_{35}H_{72}$)	*d*	99%	74.7	73.8	228.6	256.7
n-hexatriacontane ($C_{36}H_{74}$)	*e*	98%	75.8	75.5	221.5	269.2
n-heptatriacontane ($C_{37}H_{76}$)	*c*	99%	78.2	77.0	230.1	258.7
n-octatriacontane ($C_{38}H_{78}$)	*a*	99%	78.6	78.5	236.4	270.5
n-tetracontane ($C_{40}H_{82}$)	*f*	unknown	80.4	81.3	212.8	271.6
n-tetratetracontane ($C_{44}H_{90}$)	*a*	99%	86.3	86.2	223.4	273.6
n-hexatetracontane ($C_{46}H_{94}$)	*c*	99%	87.7	88.3	229.0	274.5
n-pentacontane ($C_{50}H_{102}$)	*c*	99%	91.6	92.2	213.4	276.0
n-hexacontane ($C_{60}H_{122}$)	*c*	99%	99.2	99.7	225.7	279.0

[a] Supelco, Inc., Bellefonte, PA. [b] Eastman Chemical, Rochester, NY. [c] Fluka AG, Buchs, Switzerland. [d] Ultra Scientific, Hope, RI. [e] Aldrich Chemical, Milwaukee, WI. [f] Pfaltz & Bauer, Stamford, CT.

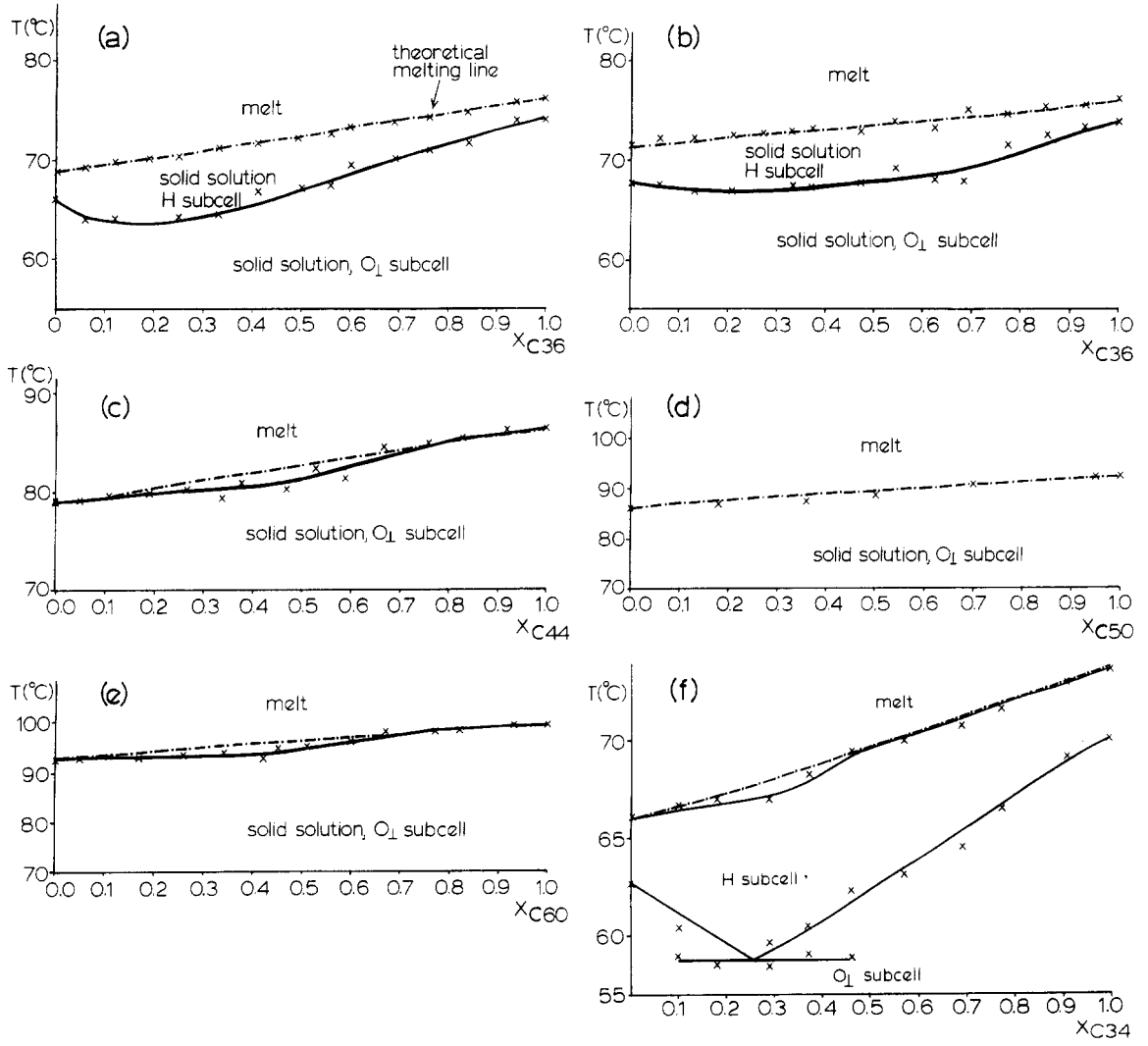

Figure 1. Binary phase diagrams for *n*-paraffin pairs that form nearly ideal solid solutions: (a) $nC_{32}H_{66}|nC_{36}H_{74}$; (b) $nC_{33}H_{68}|nC_{36}H_{74}$; (c) $nC_{38}H_{78}|nC_{44}H_{90}$; (d) $nC_{44}H_{90}|nC_{50}H_{102}$; (e) $nC_{50}H_{102}|nC_{60}H_{122}$. The first two binary compositions transform from the $O_\perp$ methylene subcell to the hexagonal H, or "rotator" packing,[40] before melting. (f) $nC_{30}H_{62}|nC_{34}H_{70}$: Partial eutectoid fractionation is found for the orthorhombic to hexagonal phase transition.

symmetry and type of layer packing for the chain axes (i.e., rectangular or oblique). In other examples, the thermodynamically most stable crystal forms of the pure compounds[2] are not necessarily the ones found for the solid solutions, so that the layer packing can change from oblique, at extreme concentrations of either component, to rectangular when the amounts of the respective ingredients become more similar.[7,8] Also a pure orthorhombic structure may possibly induce a second ingredient with a triclinic crystal structure to form a solid solution that is also orthorhombic.[6,10]

If the crystalline lamellar structure of the pure components is maintained on average for some of the intermediate solid solutions, and if the layer packing is invari-

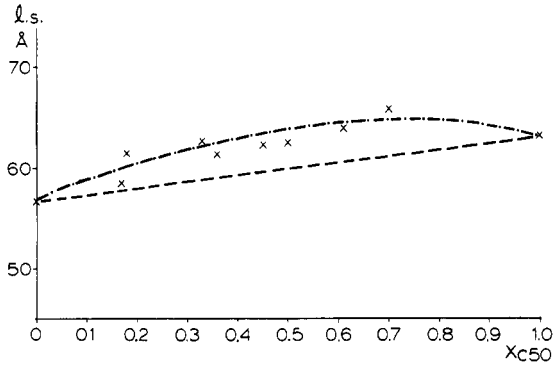

Figure 2. Plot of X-ray lamellar spacing versus binary composition for the paraffin pair $nC_{44}H_{90}|nC_{50}H_{102}$, which forms continuous solid solutions (Figure 1d).

ant for all concentrations, then relative molecular volumes are the key factor for stabilizing the solid solution[17] (i.e., by ensuring that the Gibbs free energy of this solution is lower than that of either component within the temperature range considered).[2] Although most of the experimental phase diagrams reported so far have dealt with paraffin chain lengths of 36 carbons or less, it was proposed that the stability of a solid solution in terms of chain length difference is directly dependent upon the mean chain length of its components.[20] That the solid solution is more stable than a mechanical mixture of its components has been established experimentally by diffraction and spectroscopic measurements on samples of overlapping pure paraffin lamellar crystals annealed at an elevated temperature somewhat below the melting point. In time, some sort of molecular diffusion occurs between the mechanically overlapping crystals to form the mixed chain lamellar solid.[21,22] It was postulated that this diffusion *might* be a longitudinal "flip-flop" process.[21] Fractionation has been observed when the chain length difference becomes too large and the presumed diffusion was thought to be a reversal of the solubilization mechanism observed before.[23]

Although the thermodynamic description of *n*-paraffin binary solids is clear,[1,2] the events accompanying the formation of a solid solution or, conversely, the fractionation of compounds into a eutectic solid have not been summarized in terms of a unified structural model. In this paper we extend the experimental investigation of binary phase behavior for one type of paraffin layer structure, i.e., the rectangular packing in the orthorhombic perpendicular methylene cell, to a maximum chain length of 60 carbon atoms. These data, along with those reported earlier, will be used to show the structural connection between the mixed and unmixed phases when a miscibility gap occurs below a critical temperature to cause a slow fractionation of metastable solid solutions.

Materials and Methods

***n*-Paraffins.** Commercially available normal paraffins nC_nH_{2n+2} within the chain length limits $28 \leq n \leq 60$ were obtained from the sources listed in Table I. Peak melting points determined by DSC are compared to values calculated using Broadhurst's[24] empirical formula and are found to agree reasonably well. Such agreement is not found when experimentally determined transition enthalpies are compared to values predicted by Dollhopf et al.[25] Rather, the values found by DSC are nearly independent of chain length, yielding a mean value 226.2 ± 8.4 J/g. The theoretical value for infinite extended chain length polyethylene is 293.7 J/g—thus the samples are not perfectly crystalline. This is probably related to the observation that nonplanar conformations exist in a small fraction of the molecules even at low temperatures.[26] As shown by earlier electron diffraction determinations,[27] the even paraffins all pack in the same orthorhombic structure (space group $Pca2_1$) found for the higher energy polymorph of *n*-hexatriacontane.[28] The odd-chain paraffins crystallize as the B form (space group $A2_1am$) discovered by Piesczek et al.[29] and described in greater detail in a recent electron diffraction structure analysis.[27]

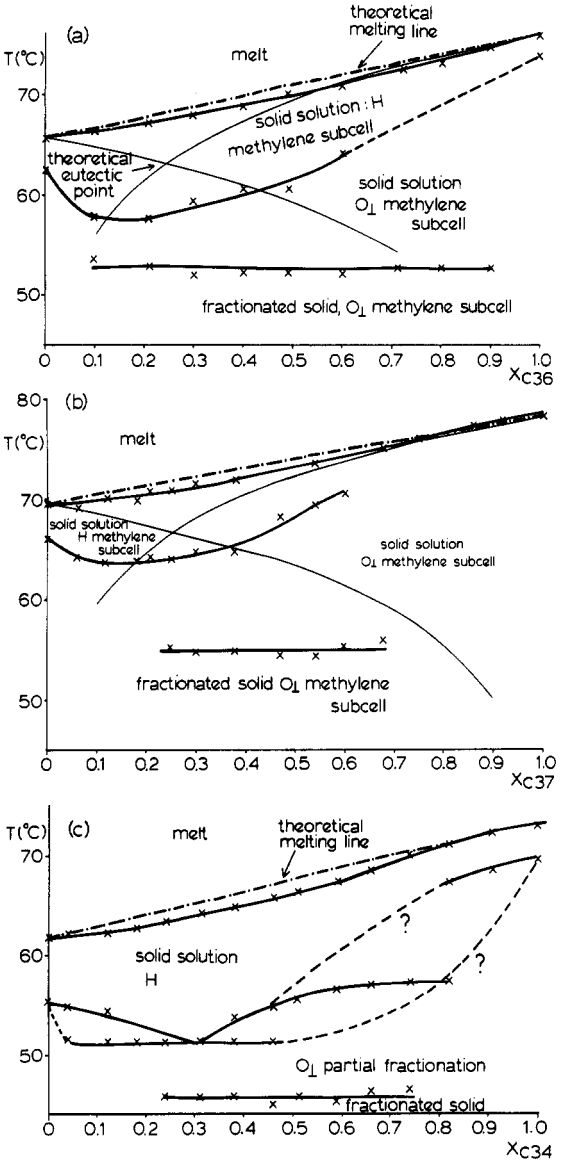

Figure 3. Phase diagrams for binary solids for which solid solutions slowly fractionate: (a) $nC_{30}H_{62}|nC_{36}H_{74}$; (b) $nC_{32}H_{66}|nC_{37}H_{76}$; (c) $nC_{28}H_{58}|nC_{34}H_{70}$. The fractionated solid at temperatures below the isotherm has been found to be incommensurate lattice structures composed of alternate sequences of pure lamellae.[23] When heated above this line a metastable solid solution is formed. The methylene subcell is still $O_\perp$, however.

Diffraction. Electron diffraction experiments were carried out at 100 kV on either a JEOL JEM-100B or a JEOL JEM-100CXII electron microscope. The samples were oriented epitaxially on benzoic acid following a procedure of Wittman et al.[30] to produce a [100] projection of the crystal structure. Diffraction spacings were calibrated with a gold Debye–Scherrer diagram photographed at the same camera length used to record the paraffin $0kl$ diffraction patterns.

Low-angle X-ray diffraction measurements were made with a homemade slit-collimated camera and a Rigaku Rotaflex rotating anode X-ray generator with a Cu Kα X-ray source operated at 40 kV and 25 mA. Diffraction patterns were detected with a position-sensitive proportional counter. Samples used for diffraction experiments were taken from DSC pans after these heating experiments were completed and centrifuged into thin-walled 1.0-mm-diameter glass capillaries.

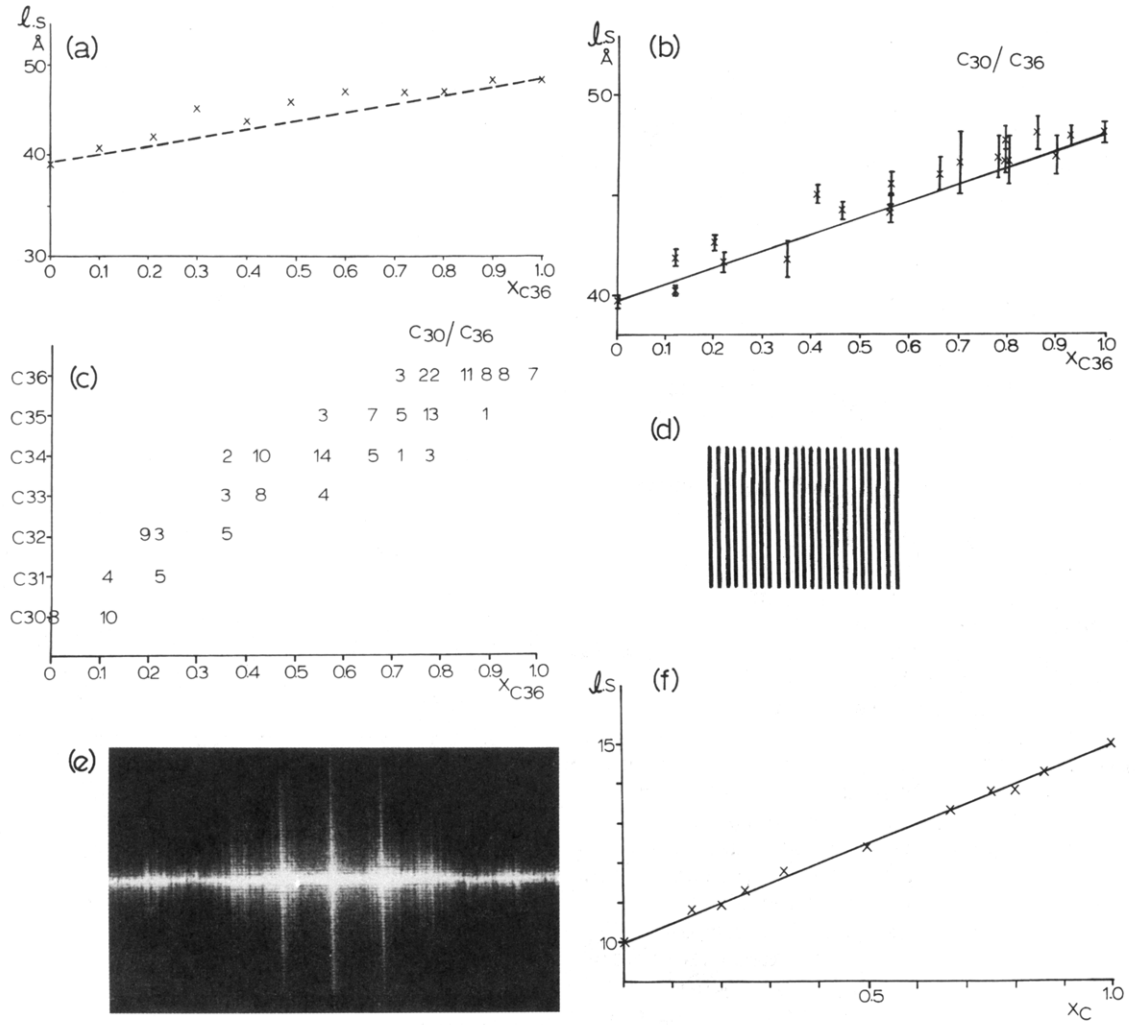

Figure 4. (a) X-ray diffraction lamellar spacings from binary solids of $nC_{30}H_{62}|nC_{36}H_{74}$, which are in the fractionated incommensurate solid represented by the phase diagrams in Figure 3. (b) Average electron diffraction lamellar spacings from $nC_{30}H_{62}|nC_{36}H_{74}$ from the repeat of the most intense reflections, corresponding to the relationship found from X-ray data in (a). (c) If the spacing of the most intense lamellar reflection is compared with the spacing of the 01*l* reflections so that these can be indexed as a paraffin crystal structure (see ref 19), then the distribution of local crystal structure with concentration is similar to that found for solid solutions.[19] (The numbers at any concentration represent how many microdomains were found on a particular grid with the crystal structure indicated on the ordinate.) (d) Model lamellar structure to simulate the phase separation in the superlattice solid. (e) The Fourier transform contains several spacings that cannot be indexed as a single lattice repeat unless a structure like a superlattice is envisioned. The concentration dependence of intense lamellar spacings is found (f) to lie on a strict Vegard's law line.

acid were obtained at 20000× direct magnification with the same electron microscope used for electron diffraction experiments and at the same accelerating voltage. Since the specimens are radiation sensitive, techniques described earlier[23] were employed to minimize beam-induced damage. The phase contrast transfer function was manipulated so that only the low-angle diffraction data could contribute to the formation of the phase contrast image of the lamellar packing. Suitably ordered areas of the resultant image, identified by optical diffraction, were scanned on an Optronics P1000 rotating drum microdensitometer to create a digitized pixel image file for later manipulation by image processing.

Light Microscopy. Observations of crystallization were made at 200× magnification a Leitz Ortholux light microscope with polarization optics. Specimens of binary melts were cooled at 5 deg/min on a Mettler FP82 hot stage regulated by a programmed FP80 control device. Upon observation of crystallization or any other change of the specimen, the temperature of this event can be recorded. After establishing where the main transitions occur, the hot stage can be held at an appropriate temperature to enable one to photograph the texture of the binary paraffin condensed state.

Differential Scanning Calorimetry. Differential scanning calorimetry of 2–4-mg samples sealed in aluminum crucibles was carried out with a Mettler TA3300 instrument, generally at a heating or cooling rate of 5 deg/min. The preweighed samples were first fused at a temperature above that of the highest melting point and then reheated after a slow cooling to room temperature. Transition enthalpies were calibrated against the value for indium and the temperature scale was adjusted to fit a polynomial curve through the known values for three metals: indium, lead, and zinc. For drawing phase diagrams, only peak values are used, including plots of solid solution melting curves (which often are made with onset and return temperature values for the main melting peak to approximate solidus and liquidus curves, respectively).

Calculations. The phase behavior of paraffin binary solids is compared to calculations based on molten solutions, which obey Raoult's law.[31] For eutectics, the well-known Schröder equations are used to calculate the liquidus curves representing the freezing point depression of an ideal liquid solution, i.e.

$$\ln x_A = -\frac{\Delta H_A}{R}\left(\frac{1}{T} - \frac{1}{T_A}\right)$$

$$\ln (1 - x_A) = -\frac{\Delta H_B}{R}\left(\frac{1}{T} - \frac{1}{T_B}\right) \quad (1)$$

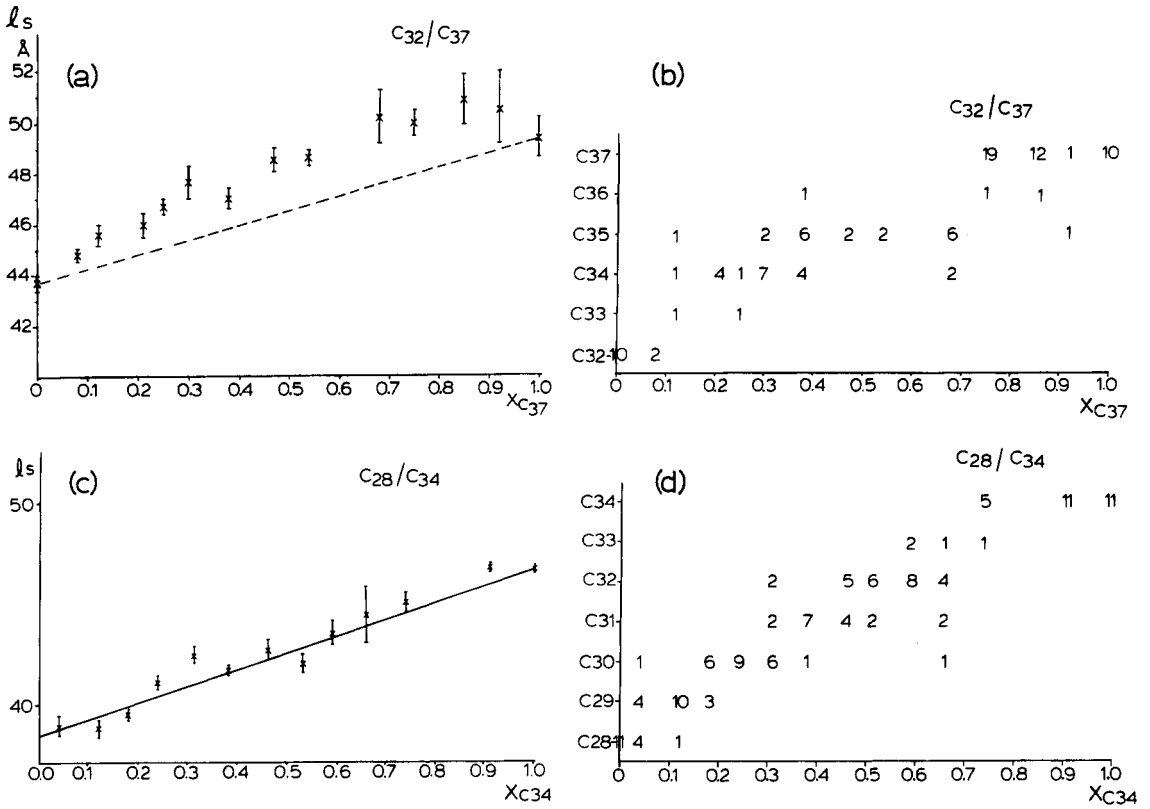

Figure 5. (a) Plot of average lamellar spacings in a concentration series of $nC_{32}H_{66}|nC_{37}H_{76}$ binary solids. Because the fractionation of the metastable solid solutions into an incommensurate solid takes at least 1 month, the electron diffraction spacings are more typical of stable solid solutions so that the intermediate spacings lie above the Vegard's law line. (b) When lamellar spacings are used to index the most intense 01l reflections, the apparent intermediate paraffin crystal structures change discontinuously with increasing concentration of C_{37}. (c) Average lamellar spacings for $nC_{28}H_{58}|nC_{34}H_{70}$, which forms the superlattice-like incommensurate solid from the metastable solid solution rather quickly. The points lie near the Vegard's law line. (d) When the major lamellar spacing is used to index the 01l reflections, the sequence of crystal structures is again found to be discontinuous with concentration.

where x_A and $x_B = 1 - x_A$ are mole fractions of the two components, ΔH_A and ΔH_B are their respective transition enthalpies, and T_A and T_B are their respective peak melting points (on the Kelvin scale). For solid solutions the melting curves were calculated by using relationships discussed by Lee,[32] i.e.

$$x_B^{(S)} = \frac{e^{-B} - 1}{e^{-A} - e^{-B}}$$
$$x_B^{(L)} = e^{-B} x_B^{(S)} \qquad (2)$$

where

$$e^{-A} = \exp\left[-\frac{\Delta H_A}{R}\left(\frac{1}{T} - \frac{1}{T_A}\right)\right]$$
$$e^{-B} = \exp\left[-\frac{\Delta H_B}{R}\left(\frac{1}{T} - \frac{1}{T_B}\right)\right]$$

Here $x_B^{(S)}$ and $x_B^{(L)}$ respectively refer to mole fractions for solidus and liquidus curves. Since we are comparing the calculation to experimental peak values, we use the average mole fraction $\bar{x}_B = (1/2)(x_B^{(L)} + x_B^{(S)})$. For these calculations, experimental rather than theoretical values are used for melting points and transition enthalpies of the pure components, as listed in Table I. No corrections for nonideal behavior[31,32] were made for reasons made clear below.

Although the crystal structure of an incommensurate lamellar chain packing associated with some of the fractionated solids discussed below has been reported in an earlier paper, further tests of the low-angle diffraction data for a continuous composition series of the two components were made with simplistic lamellar packing arrays. Such models were scanned with an Optronics P1000 rotating drum microdensitometer to create a digital pixel file in a VAX 8600 computer that could be manipulated by programs (e.g., fast Fourier transform) in a image processing program package IMAGIC.[33] These models were compared to Fourier transforms computed from similarly digitized electron microscope images.

Results

For the binary paraffin compositions presented below, three types of solid-state structures were formed: solid solution, fractionated solid solution, and the eutectic structure. For the former and latter, phase diagrams are very well explained by the ideal theory using eq 1 and 2. The intermediate, slowly fractionated state leads to insights into the transition from cosoluble to fully phase-separated solids as a function of relative molecular volumes.

Solid Solutions. In a sequence of mean carbon chain lengths, stable solid solutions have been formed for the binary compositions $nC_{32}H_{66}|nC_{36}H_{74}$, $nC_{33}H_{68}|nC_{36}H_{74}$, $nC_{38}H_{78}|nC_{44}H_{90}$, $nC_{44}H_{90}|nC_{50}H_{102}$, and $nC_{50}H_{102}|nC_{60}H_{122}$. (The first two paraffin pairs were redetermined since the calorimetric experiment in the earlier publication was somewhat less accurate than possible on the newer apparatus.) Theoretical melting curves for each binary paraffin solid calculated by eq 2 are in very close agreement to the experimental data (Figure 1) with some slight deviation of the curves occurring for solids composed of longer chain components. There are no deviations from ideal mixing found for the odd/even paraffin solution, in agreement with our earlier data[18] and also data presented in earlier studies, which indicate continuous solubility of such compounds.[11]

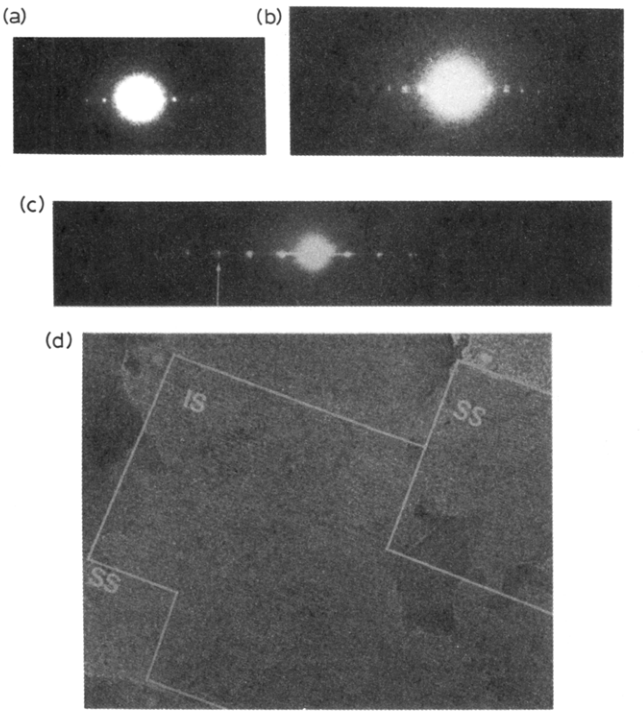

Figure 6. Sequence of electron diffraction patterns as a metastable solid solution of $n\mathrm{C}_{32}\mathrm{H}_{66}|n\mathrm{C}_{37}\mathrm{H}_{76}$ (composition $X_{\mathrm{C37}} = 0.75$) is allowed to equilibrate: (a) The initial patterns have a single lamellar spacing with limited spatial frequency resolution, typical of a mixed-chain lamellar packing.[18] (b) Accompanying the appearance of a new endotherm in DSC scans, the resolution of the lamellar $00l$ line increases, indicating that the lamellar packing is more ordered. (c) Finally one finds several lamellar spacings characteristic of a superlattice-like structure (splitting shown by arrow). (d) Domains of a superlattice-like incommensurate solid growing in the initial solid solution found in an electron micrograph of epitaxially oriented $n\mathrm{C}_{30}|n\mathrm{C}_{36}$ (IS, fractionated lattice; SS, solid solution).

In our earlier electron diffraction determination for $\mathrm{C}_{32}|\mathrm{C}_{36}$ and $\mathrm{C}_{33}|\mathrm{C}_{36}$,[18] it was found that average lamellar spacings for intermediate mole fractions of binary solid solutions lie somewhat above the Vegard's law line joining the lamellar spacings of the pure components, as found also in earlier powder X-ray studies of bulk samples.[12] A representative plot of lamellar spacings for one of the longer chain solid solutions, i.e., $n\mathrm{C}_{44}\mathrm{H}_{90}|n\mathrm{C}_{50}\mathrm{H}_{102}$, is shown in Figure 2 to have the same behavior. The significance of this average lamellar spacing in terms of crystal structure was discussed in a recent paper,[19] where it was shown that there is no continuity of solid solution behavior in terms of *unit cell* symmetry. The same behavior is noted in recent electron diffraction measurements on $n\mathrm{C}_{50}\mathrm{H}_{102}|n\mathrm{C}_{60}\mathrm{H}_{122}$ solid solutions (Zhang, W. P.; Dorset, D. L., manuscript in preparation).

Although the effect of mean chain length on the formation of stable solid solutions from binary paraffin compositions with a certain chain length difference will be discussed in detail below, the first signs of instability in such systems might be indicated by the phase diagram in Figure 1f. In the previous diagrams for paraffins with the orthorhombic to hexagonal "rotator" phase transition, it is clear that the experimental curve connecting the temperatures of the two pure components is nonideal since at intermediate compositions the pretransition temperature is appreciably lowered. For the phase diagram of $n\mathrm{C}_{30}\mathrm{H}_{62}|n\mathrm{C}_{34}\mathrm{H}_{70}$ in Figure 1f, some sign of fractionation is found in this orthorhombic to hexagonal rotator transition curve since part of a isothermal solidus curve is detected on either side of a eutectic point. The phase separation here is probably a fractionation of solid solutions. A different type of fractionation is discussed in the following section.

Miscibility Gap. Earlier[23] we found one binary solid $n\mathrm{C}_{30}\mathrm{H}_{62}|n\mathrm{C}_{36}\mathrm{H}_{74}$ for which a metastable solid solution fractionates after standing, e.g., for 2 days at room temperature. We have redetermined its phase diagram as shown in Figure 3a. Analysis of the experimentally found endothermic transitions in terms of eq 1 and 2 above reveals that the highest temperature transition to the melt lies very close to the melting point line of an ideal solid solution. The eutectic solidus line predicted from eq 1, however, is not at all close to the isotherm that was thought earlier to correspond to a structural transformation from the incommensurate solid to a solid solution.[23] (The incommensurate solid, which is a random sequence of pure paraffin lamellae, was incorrectly termed a superlattice in the earlier communication.[23] For simple molar ratios, it is expected that this solid may be superlattice-like, however, with a nearly regular lamellar sequence.) Although all the superlattice-like lamellar reflections could be detected by electron diffraction, low-angle X-ray diffraction patterns from equilibrated specimens in a concentration series contain one major row of low-angle peaks corresponding only to the most intense reflections, the spacing of which lies near to a theoretical Vegard's law line (Figure 4a). (This row of reflections often has a regular repeat for several orders, indicative of the solid solution from which the fractionated arrays was formed.) For the sake of comparison, the spacings, determined from the most intense lamellar reflections in the incommensurate solid electron diffraction patterns[23] for binary composition of $n\mathrm{C}_{30}\mathrm{H}_{62}|n\mathrm{C}_{36}\mathrm{H}_{74}$, are shown to produce a similar result (Figure 4b), in that their average values lie very near to the Vegard's law line. If these spacings are used to index the $01l$ reflections in the $0kl$ electron diffraction patterns to find a local average crystal structure for a parent solid solution (see ref 19), then the compositional dependence of crystal structure type is again discontinuous (Figure 4c) with alternations of unit cell symmetry similar to those found earlier for true solid solutions.[19] (Briefly, indices of the two strong $01l$ paraffin reflections corresponding to the 011 subcell planes of the polymethylene zigzag are related to the carbon number $\mathrm{C}_n\mathrm{H}_{2n+2}$ of the average crystal structure by $l = n, n + 2$.) Comparison to a parent solid solution is justified since this is the precursor to the fractionated solid and, indeed, coexists with it, as we shall see below.

If one uses model lamellar arrays to construct an incommensurate solid (Figure 4d) and uses their Fourier transforms (Figure 4e) to evaluate the position of the most intense reflection with lamellar concentration, then the relationship can be shown to be strictly linear (Figure 4f) in accord with the exact Vegard's law behavior observed for these solids, which is distinct from the behavior found for solid solutions (see Figure 2). The absence of superlattice-type lines in the low-angle X-ray diffraction patterns is undoubtedly due to the low spatial coherence of typical X-ray sources compared to the nearly parallel illumination used in electron diffraction, which corresponds to a large spatial coherence value.[34]

A second paraffin pair composed of an even/odd mixture, i.e., $n\mathrm{C}_{32}\mathrm{H}_{66}|n\mathrm{C}_{37}\mathrm{H}_{76}$, has been found to exhibit similar phase behavior (Figure 3b) although the initial time for appearance of the new endotherm in the DSC scan is somewhat longer than for the even/even system just discussed, with this transition occurring within 1 week. Again the observed melting line lies close to the one cal-

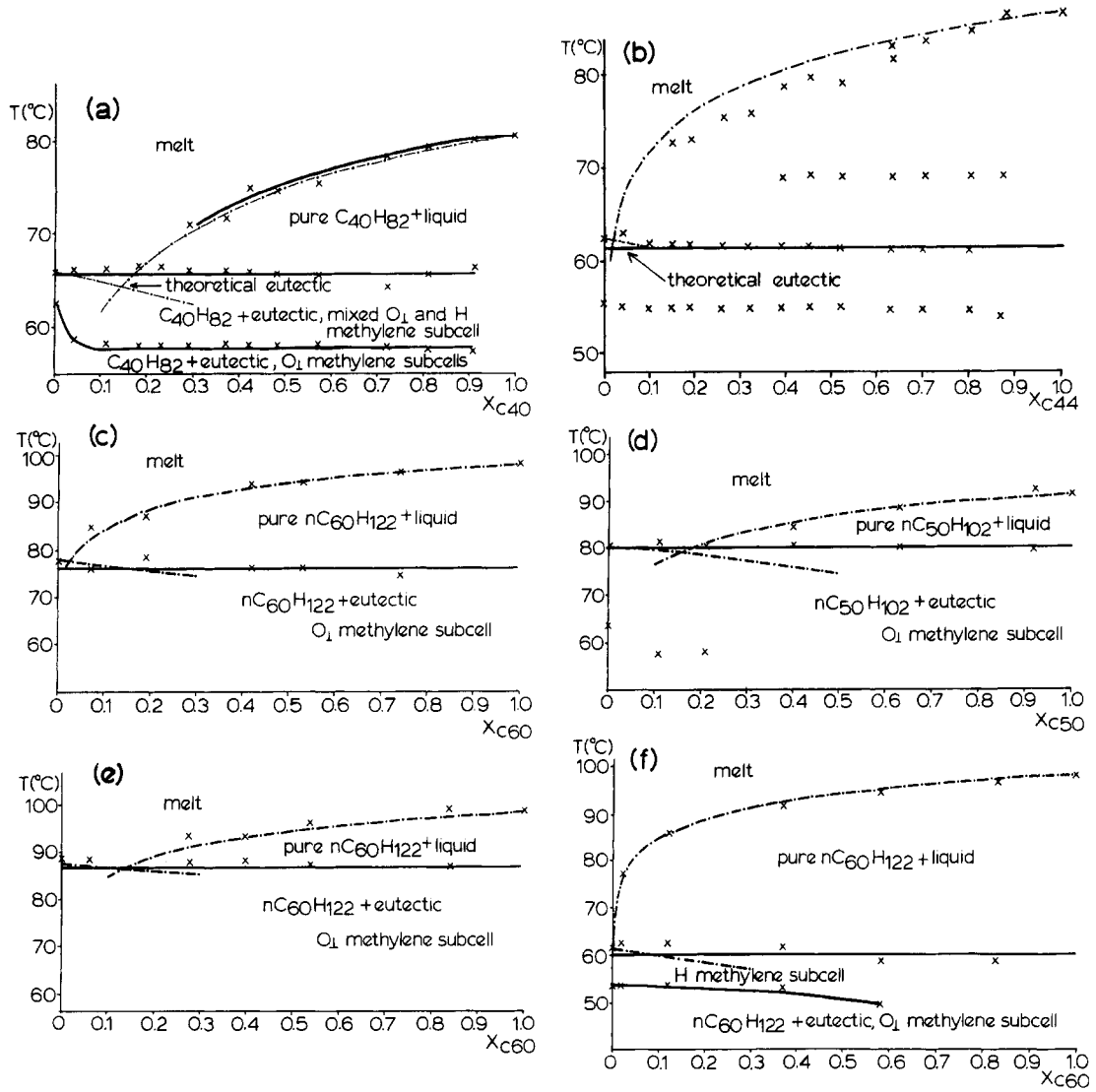

Figure 7. Phase diagrams from true paraffin eutectics: (a) $nC_{30}H_{62}|nC_{40}H_{82}$; (b) $nC_{28}H_{58}|nC_{44}H_{90}$; (c) $nC_{38}H_{78}|nC_{60}H_{122}$; (d) $nC_{40}H_{82}|nC_{50}H_{102}$; (e) $nC_{46}H_{84}|nC_{60}H_{122}$; (f) $nC_{28}H_{58}|nC_{60}H_{122}$.

culated for an ideal solid solution and the predicted eutectic solidus is not close to the isothermal transition observed in our DSC scans. For samples just epitaxially orientated on benzoic acid, the average lamellar spacings lie above the Vegard's law line (Figure 5a) as is found for stable solid solutions. Even though the new endotherm appears after a week's standing in these samples, the electron diffraction patterns continue to be typical of a stable solid solution, i.e., there is only one lamellar spacing. Indexing of $01l$ reflections using the lamellar spacing again demonstrates the discontinuity of intermediate crystal forms with two or more unit cell symmetries and/or lamellar spacings found for any given intermediate composition (Figure 5b). Preliminary experiments have also been carried out for the solids composed of $nC_{30}H_{62}|nC_{35}H_{72}$, which had been found by Mazee[11] to fractionate into a superlattice-like solid. The phase behavior is similar to the two examples presented here, although the fractionation time is much longer. Yet another combination, viz., $nC_{28}H_{58}|nC_{34}H_{70}$, begins to fractionate within 1 day at room temperature. The phase diagram is shown in Figure 3c. Since this combination fractionates very quickly, the spacings of intermediate strong lamellar reflections lie near the Vegard's law line (Figure 5c) and the crystal structure symmetries for the parent solid solutions again change discontinuously with concentration (Figure 5d).

From the above comparisons of experimental data to thermodynamic computations, it is clear that the isotherms in Figure 3 do not correspond to a true eutectic. Although it was not clear from the initial study on $nC_{30}|nC_{36}$, the first appearance of the new isothermal transition does not itself correspond to the occurrence of a superlattice-like structure. For the binary solids of $nC_{32}|nC_{37}$, the isotherm can appear within 1 week of standing at room temperature but the epitaxially crystallized samples will still produce electron diffraction patterns after 1 month that have no sign of superlattice-like spacings (Figure 6b). The slower growth of the incommensurate solid as separate domains can also be visualized in electron micrographs of $nC_{30}|nC_{36}$ (Figure 6d) where such regions are found to coexist with the solid solution. In terms of the initial rearrangement of the solid to produce a better ordered solid solution, the growth of the fractionated solid takes a very long time (weeks, months, years). After, e.g., 1 year's equilibration, a transition enthalpy on the isotherm for $nC_{30}H_{62}|nC_{36}H_{74}$ does not differ from that of samples equilibrated for only 1 week, although the peak temperature of this transition increases from ca. 49 to ca. 54 °C.

Eutectic. Earlier,[23] the structure of a eutectic between $C_{30}H_{62}$ and $C_{40}H_{82}$ was discussed and electron diffraction patterns indicated the presence of a superlattice-

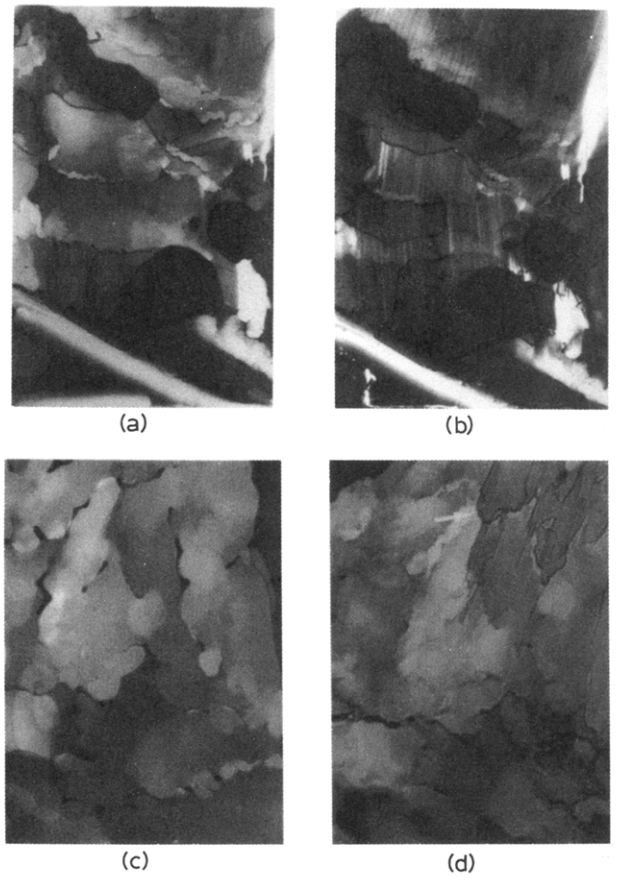

Figure 8. Observation of eutectic solidification in a polaring light microscope. For the binary melt of $nC_{30}H_{62}|nC_{40}H_{82}$, it is easy to observe (a) the primary crystallization of nC_{40}-rich solid when the liquidus curve is crossed upon cooling, but the secondary crystallization is more difficult to locate (b). In cooled co-melts of $nC_{28}H_{58}|nC_{44}H_{90}$, on the other hand, it is easy to detect both the primary (c) and secondary (d) crystallization at the liquidus and solidus curve, respectively. (Note localized overgrowth of nC_{44} indicated by arrow.)

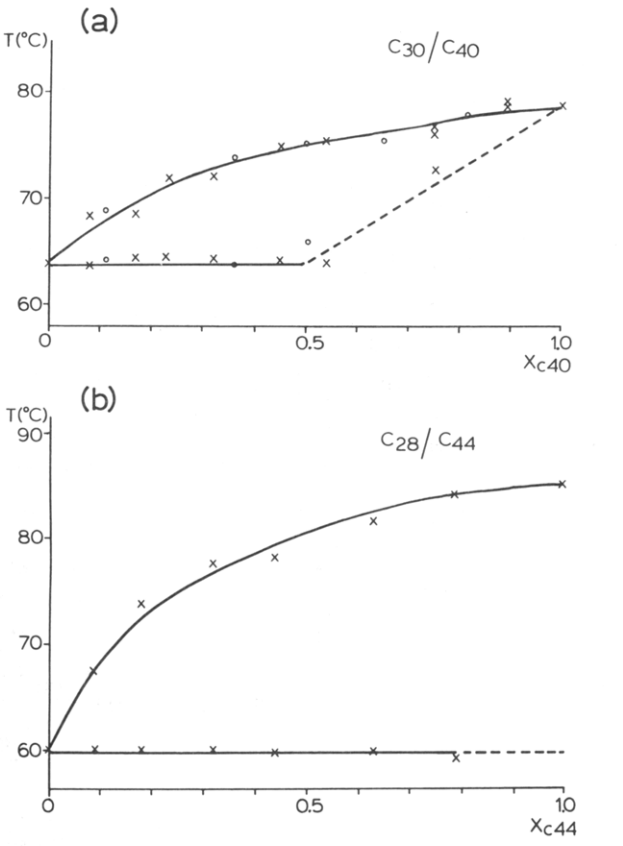

Figure 9. Plots of the crystallization temperatures determined with a heating stage on an optical microscope for the two eutectic systems in Figure 8 reveal a difference in their solidification behavior. (Samples were cooled from the melt.) (a) $nC_{30}H_{62}|nC_{40}H_{82}$: the solidus line is isothermal over a limited concentration region; there must be metastable solid solubility at high concentrations of C_{40}. (b) $nC_{28}H_{58}|nC_{44}H_{90}$: Here the liquidus and solidus curves correspond to the phase diagram in Figure 7b. There is no metastable cosolubility of these paraffins in the solid state.

like structure, similar to that of the slowly fractionating system described above, in addition to domains of the pure higher melting component. The phase diagram has been redetermined and comparison to theoretical calculation shows (Figure 7a) that the observed and calculated liquidus curves on the higher melting side of the eutectic lie close to one another. The predicted eutectic solidus is only 2 °C away from the observed isotherm. A similar agreement between calculated and observed behavior is found for other binary eutectics (Figure 7b–f).

Although the phase diagrams in Figure 7 appear to represent substances that are totally phase separated in the solid state, an examination of the crystallization behavior for rapidly cooled melts in a light microscope reveals that metastable solid solutions can exist for large concentrations of the higher molecular weight components when the chain length difference is not too large. For example, the primary crystallization at the liquidus curve for $nC_{30}H_{62}|nC_{40}H_{82}$ is easily observed (Figure 8a) but the secondary crystallization point is hard to locate precisely at large x_{c40} (Figure 8b), so that the observed isothermal region of the solidus curve is somewhat limited (Figure 9a). This is contrasted with the cooling behavior of $nC_{28}H_{58}|nC_{44}H_{90}$ melts for which both primary and secondary crystallizations are easily identified in the light microscope (Figure 8c,d), so that a plot of the crystallization temperatures (Figure 9b) resembles the phase diagram in Figure 7b. It is apparent that two types of eutectic solid are formed depending on the existence of a metastable solid solution in the rapidly cooled melt.

When the chain length difference between the paraffins is small enough to cause the formation of a metastable solid solution, the eutectic solid again consists of a superlattice-like incommensurate solid. For compositions rich in either component, strong electron diffraction lamellar reflections appear to originate from respective zones of pure paraffins. A third lamellar reflection with spacings between these two values occurs for intermediate compositions and denotes the existence of the incommensurate solid that forms on crossing the isothermal solidus line. However, the contribution from domains of the pure higher melting paraffin is always present in these patterns for a large concentration range of this component in the melt. Thus, in optical transforms of electron microscope lattice images of these solids, the lamellar diffraction peaks from the incommensurate solid and the higher melting component can be separated by Fourier peak filtration by using appropriate masks to bandpass either set of reflections in reciprocal space as already discussed.[23] More recent electron micrographs of this solid clearly show the sharp grain boundary between the pure $nC_{40}H_{82}$ component and the incommensurate solid.[35] The dependence of the intermediate lamellar Bragg spacing on paraffin composition in the incommensurate solid, however, was not easy to discern because of a rather larger standard deviation in the earlier measurements.[23] The X-ray lamellar spacings for the binary mixture

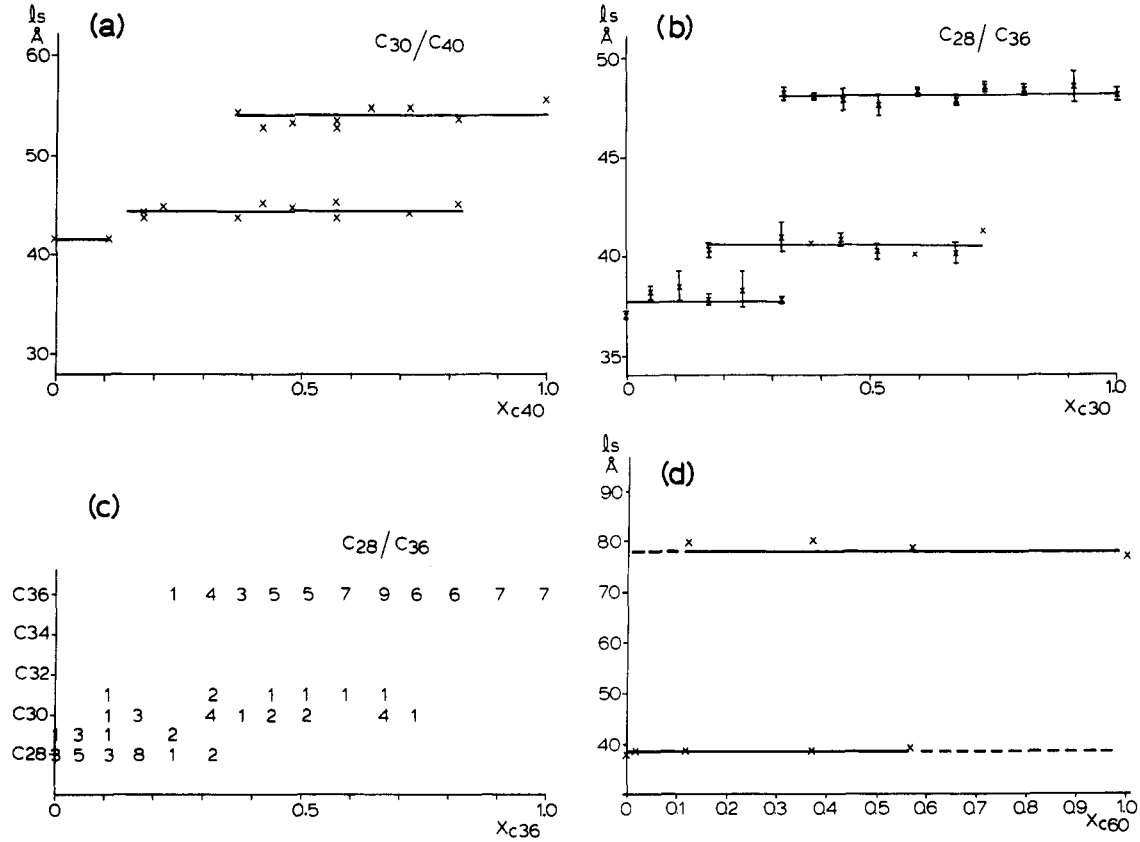

Figure 10. X-ray lamellar spacings for eutectic paraffin solids (a) $nC_{30}H_{62}|nC_{40}H_{82}$ with limited cosolubility. (b) Averaged electron diffraction lamellar spacings from binary solids of $nC_{28}H_{58}|nC_{36}H_{74}$, with behavior similar to the $nC_{30}H_{62}|nC_{40}H_{82}$ binaries. (c) When the local crystal structures are determined, one finds most often domains of pure $C_{28}H_{58}$ or $C_{36}H_{74}$ at concentration extremes and, at intermediate concentrations, a parent solid solution structure of $nC_{30}H_{62}$ or $nC_{31}H_{64}$, which fractionates into the superlattice-like structure. (d) $nC_{28}H_{58}|nC_{60}H_{122}$ with no cosolubility of components. Such a eutectic separation of pure components is also found for, e.g., $nC_{28}H_{58}|nC_{44}H_{90}$.

$nC_{30}H_{62}|nC_{40}H_{42}$ (Figure 10a) indicate that the intermediate spacing is independent of concentration, in contrast to the case of the fractionated solid solutions discussed above. Similar behavior can be shown for the binary composition of $nC_{28}H_{58}|nC_{36}H_{74}$, which also forms a eutectic. Electron diffraction patterns from epitaxially crystallized samples contain the same sort of superlattice-like spacings found for $nC_{30}H_{62}|nC_{40}H_{82}$. A plot of the average lamellar spacings (Figure 10b) shows the overlap of three crystalline regions, i.e., the two pure components at respective extremes of concentration and the intermediate superlattice-like solid of nearly constant composition formed from the metastable solid solution. If the lamellar spacings are used to index the $01l$ reflections as done above, then the local paraffin crystal structures are those of either the primary pure component or the secondary incommensurate solid. The latter indices would resemble those from a solid solution of nearly constant composition and crystal structure (Figure 10c).

The second type of solid obtained when the chain length difference is too great to allow formation of a metastable solid solution is one where pure paraffins exist as separate crystals with no evidence for any superlattice-type structure. Electron diffraction patterns from epitaxially oriented binary compositions of $nC_{28}H_{58}|nC_{44}H_{90}$, for example, indicate that the domains of pure paraffin of either composition are relatively large. This behavior is exactly the same as observed for another totally phase separated system of long chain molecules, viz., *n*-hexatriacontane/stearyl stearate,[36] for which the primary and secondary crystallization steps are also easily observed in the light microscope.

It is also interesting to note the phase behavior for $C_{28}H_{58}|C_{60}H_{122}$ (Figure 7f). It was suggested by Bonsor and Bloor[4] that a paraffin with half the lamellar spacing of a second paraffin may be stabilized in a solid solution of the longer with two of the shorter molecules aligning along one longer molecule in a lamella. In this study binary compositions were quickly quenched from the melt into liquid nitrogen in an attempt to stabilize such a mixed lamellar solid. In all cases, the phase diagrams are identical with those formed for preparations slowly cooled from the melt. Again it is shown that the lamellar X-ray reflections from the fractionated solid represent spacings from only the two pure components with no evidence for a superlattice-like intermediate form (Figure 10d).

Discussion

Experimental calorimetric data from binary paraffin solids that form either solid solutions or eutectics can be used to construct phase diagrams that match very well theoretical calculations based on ideal solution theory. This is understandable since there is only one type of intermolecular interaction due to van der Waals forces and because the molecular volume differences are not large in most cases. (However, see Figure 7c,f). Similar agreement to ideal theory had been noted earlier for other binary paraffins.[1,2] It is also apparent that the molecular volume difference tolerated in a stable solid solution is nearly the value predicted by Matheson and Smith.[20] Our data indicate that the line might be shifted to slightly higher values of the minimum carbon number and the slope of their empirical curve may change slightly (Fig-

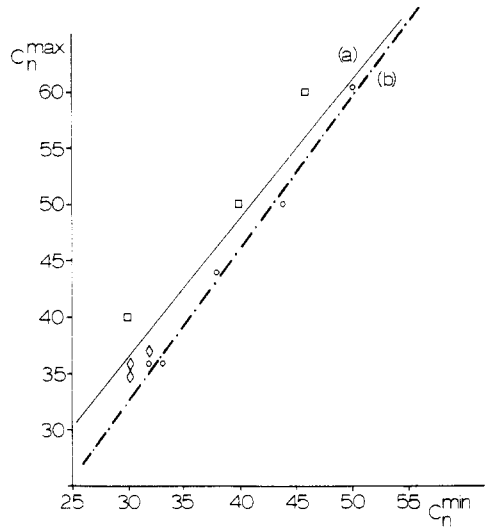

Figure 11. Characteristics of absolute mean chain length and chain length difference for the formation of a stable solid solution. In an earlier study,[20] the minimum and maximum chain lengths allowed in a solid solution (○) were found to be described by the line $C_n^{max} = 1.224C_n^{min} - 0.411$, indicated by curve a in this graph. However, metastable solid solutions (◇) are found at positions to the right of this curve, in a region where only stable solid solutions should exist. All eutectic compositions (□) found in this study lie to the left of this line as expected. If the positions of stable solid solutions found in this study (○) are used for a least-squares calculation, curve b, described by the equation $C_n^{max} = 1.33C_n^{min} - 7.22$, is derived. The true boundary curve is slightly to the left of this line.

ure 11). This observation is based on the existence of metastable solid solutions near their theoretical line, which separate after several days (or weeks or months) of standing.

The occurrence of the fractionating metastable solid solutions when the molecular volume difference becomes too large is significant for the understanding of molecular dynamics during phase transitions in terms of a structural model. As shown in the sequence of diffraction patterns in Figure 6, there are three different structures that can be formed as a metastable solid solution is allowed to equilibrate at room temperature. First, the existence of the solid solution itself it shown by the occurrence of a $00l$ spacing in the electron diffraction pattern from a single average lamellar spacing (Figure 6a). Attenuation of the resolution for these reflections is a consequence of the approximately Gaussian falloff of chain carbon atom occupancies at the interlamellar interfaces due to the comixture of different chain lengths within a lamella, as well as chain end defects. Such a model was used quantitatively to determine the structure of a 1:1 $n\mathrm{C_{32}H_{66}}|n\mathrm{C_{36}H_{74}}$ solid solution in projection.[18] The other end point is the superlattice-like incommensurate solid structure indicated by the diffraction pattern in Figure 6c. A model which seems to satisfy the diffraction data is a random alternation of pure phase-separated lamellae that are in exact register across their methyl end planes.[23] The link between these two structures is indicated by the diffraction pattern in Figure 6b.

While it is tempting to explain the transition from the solid solution in Figure 6a to the incommensurate solid in Figure 6c by a longitudinal diffusion across the methyl end plane boundary, it is difficult to imagine an intermediate structural model that would account for the increased lamellar resolution found in Figure 6b if such a diffusion mechanism were to take place. A simple-minded interpretation of this diffraction pattern would lead to a model where the chain end order in single bicomponent lamellae is more perfect so that, on the average, the occupancies of all atoms near the lamellar interface are near 1.0. Formation of the superlattice-like structure therefore requires more time than the initial event, which involves a reordering of individual lamellae. How this occurs, exactly, will be the subject of vibrational spectroscopy and neutron diffraction experiments. The growth of this solid probably causes the increased transition temperature of the isotherm noted above. It is apparent, however, that this process is typical of other binary solid solutions that are held below a critical temperature to create a miscibility gap.[37] Although the slowly appearing endotherms form an isothermal line, this is in fact the binodal solidus line, which often has a parabolic shape in other binary systems.

When the chain length difference becomes great enough for eutectic phase separation to occur, i.e., when the critical temperature for phase separation crosses the melting line, a superlattice-like incommensurate solid is formed as the secondary solid if a metastable solid solution is initially formed from the rapidly cooled melt. Unlike the slowly fractionated solid solutions at the miscibility gap, however, it is formed more quickly and has an invariant structure with changing concentration. If an intermediate solid solution is not formed, then the two components crystallize separately in the eutectic solid. This is because the eutectic point is located virtually at zero concentration for the longer chain component. Thus, as the melt is cooled, the higher molecular weight species is almost completely crystallized between initial crossing of the liquidus curve and just above the solidus. The second paraffin component crystallizes onto the first at the solidus curve as an overgrowth that undoubtedly is epitaxially directed by a match of identical methyl end planes in the opposing (001) faces. As stated before for the *n*-hexatriacontane/stearyl stearate example,[36] this is a trivial example of a lamellar eutectic that is constrained by growth conditions.

Lamellar eutectics are also well-known in metallurgy. Gordon[37] discusses their formation in terms of a metastable extension of liquidus curves in the vicinity of the eutectic point to an undercooled temperature so that each component alternately crystallizes out as the effective undercooling oscillates back and forth on either side of the eutectic point. Like the paraffin eutectics, there is often an epitaxial relationship between the lamellae,[38] and, in the case of eutectoid solids, the lamellar repeats are smaller due to constrained diffusion in the solid state.[37] While the similarity to the paraffin eutectics is compelling, it is apparent from our work that the growth mechanism is quite different from that of the eutectic alloys. First, the eutectic point is generally at a concentration extreme rather than somewhere between the two pure component concentrations, thus making such an oscillatory growth mechanism improbable. Second, superlattice-like structures are found only when a metastable solid solution is formed upon initial crystallization, either when solid solutions are cooled below a critical temperature or when a eutectic is formed from solid solutions. When a miscibility gap is reached, the fractionation is diffusion controlled and takes a long time to achieve equilibrium separation. Alternate stacking of lamellae is the easiest way to achieve a total phase separation over the shortest diffusion path.

Finally it can be seen that a gradual change in the type of *crystalline array* occurs between the stable solid solutions and the fully separated eutectics as the chain length

difference is slowly increased. Given the structural similarity of all members of the homologous paraffin series used to construct the binary solids, however, it is not possible to speak of a "mechanical" mixture of components when these are totally phase separated, since all associations of crystal faces can lead to exact epitaxial relationships. So-called "anomalous" relationships between components of a eutectic occur only when the two interacting crystal faces are incompatible, as shown in our recent study of paraffin/aromatic solids[39] (see also references cited in this work). On the other hand, when epitaxial relationships are allowed by the match of crystal faces and the sequence of crystallization, they will occur to lower the energy at the crystal–crystal interface.

Acknowledgment. Research described here was supported by a grant from the National Science Foundation (DMR 86-10783). I am especially grateful to Dr. Robert G. Snyder and Dr. Cynthia Goh for helpful discussion of this work and communication of the results from spectroscopic measurements in progress on the metastable solid solution systems. Dr. Andrew Massalski is thanked for translating two of the Russian articles. Gail Karet is thanked for determining the phase diagram of the quickly quenched $C_{28}|C_{60}$ binaries.

Registry No. Polyethylene, 9002-88-4.

References and Notes

(1) Asbach, G. I.; Kilian, H. G.; Stacke, F. *Colloid Polym. Sci.* **1982**, *260*, 151.
(2) Asbach, G. I.; Kilian, H. G. *Ber. Bunsenges. Phys. Chem.* **1980**, *74*, 814.
(3) Asbach, G. I.; Geiger, K.; Wilke, W. *Colloid Polym. Sci.* **1979**, *257*, 1049.
(4) Bonsor, D. H.; Bloor, D. *J. Mater. Sci.* **1977**, *12*, 1559.
(5) Craievich, A.; Doucet, J.; Denicolo, I. *J. Phys. (Paris)* **1984**, *45*, 1473.
(6) Denicolo, I.; Craievich, A. F.; Doucet, J. *J. Chem. Phys.* **1984**, *80*, 6200.
(7) Kitaigorodskii, A. I.; Mnyukh, Yu. V.; Nechitailo, N. A. *Sov. Phys. Crystallogr.* **1958**, *3*, 303.
(8) Lüth, H.; Nyburg, S. C.; Robinson, P. M.; Scott, H. G. *Mol. Cryst. Liq. Cryst.* **1974**, *27*, 337.
(9) Maroncelli, M.; Strauss, H. L.; Snyder, R. G. *J. Phys. Chem.* **1985**, *89*, 5260.
(10) Mazee, W. M. *Anal. Chim. Acta* **1957**, *17*, 97.
(11) Mazee, W. M. (*Polym. Prepr. (Am. Chem. Soc., Div. Pet. Chem.)* **1958**, *3* (4), 35.
(12) Mnyukh, Yu. V. *Zh. Strukt. Khim.* **1960**, *1*, 370.
(13) Nechitailo, N. A.; Rozenberg, L. M.; Terent'eva, E. M.; Topchiev, A. V. *Dokl. Akad. Nauk SSSR* **1957**, *116*, 613.
(14) Nechitailo, N. A.; Topchiev, A. V.; Rozenberg, L. M.; Terent'eva, E. M. *Russ. J. Phys. Chem.* **1960**, *34*, 1268.
(15) Retief, J. J.; Engel, D. W.; Boonstra, E. G. *J. Appl. Crystallogr.* **1985**, *18*, 156.
(16) Topchiev, A. V.; Nechitailo, N. A.; Rozenberg, L. M.; Terent'eva, E. M. *Dokl. Akad Nauk SSSR (Engl. Transl.)* **1957**, *117*, 1053.
(17) Kitaigorodskii, A. I. *Organic Chemical Crystallography*; Consultants Bureau: New York, 1961; pp 231 ff.
(18) Dorset, D. L. *Macromolecules* **1985**, *18*, 2158.
(19) Dorset, D. L. *Macromolecules* **1987**, *20*, 2782.
(20) Matheson, R. R., Jr.; Smith, P. *Polymer* **1985**, *26*, 288.
(21) Ungar, G.; Keller, A. *Colloid Polym. Sci.* **1979**, *257*, 90.
(22) Zerbi, G.; Piazza, R.; Holland-Moritz, K. *Polymer* **1982**, *23*, 1921.
(23) Dorset, D. L. *Macromolecules* **1986**, *19*, 2965.
(24) Broadhurst, M. G. *J. Res. Natl. Bur. Stand.* **1966**, *70A*, 481.
(25) Dollhopf, W.; Grossmann, H. P.; Leute, U. *Colloid Polym. Sci.* **1981**, *259*, 267.
(26) Maroncelli, M.; Qi, S. P.; Strauss, H. L.; Snyder, R. G. *J. Am. Chem. Soc.* **1982**, *104*, 6237.
(27) Dorset, D. L. *J. Polym. Sci., Polym. Phys. Ed.* **1986**, *24*, 79.
(28) Teare, P. W. *Acta Crystallogr.* **1959**, *12*, 294.
(29) Piesczek, W.; Strobl, G. R.; Malzahn, K. *Acta Crystallogr.* **1979**, *B30*, 1278.
(30) Wittman, J. C.; Hodge, A. M.; Lotz, B. *J. Polym. Sci., Polym. Phys. Ed.* **1984**, *21*, 2495.
(31) Lewis, G. N.; Randall, M. *Thermodynamics*; 2nd ed.; McGraw-Hill: New York, 1961; pp 280 ff; Revised by K. S. Pitzer and L. Brewer.
(32) Lee, A. G. *Biochem. Biophys. Acta* **1978**, *507*, 433.
(33) Heel, M. v.; Keegstra, W. *Ultramicroscopy* **1981**, *7*, 113.
(34) McLaren, A. C.; MacKenzie, W. S. *Phys. Stat. Sol.* **1976**, *A33*, 491.
(35) Zhang, W. P.; Dorset, D. L. *Proceedings of the Electron Microscopy Society of America*; 47th Ann. Meeting; San Francisco Press: San Francisco, 1989; p 702.
(36) Dorset, D. L. *J. Polym. Sci. B, Polym. Phys. Ed.* **1989**, *27*, 1161.
(37) Gordon *Principles of Phase Diagrams in Material Systems*; McGraw-Hill: New York, 1968; pp 148 ff.
(38) Kerr, H. W.; Lewis, M. H. In *Advances Epitaxy and Endotaxy*; Schneider, H. D.; Ruch, V., Eds.; VEB Deutscher Verlag für Grundstoffindustrie; Leipzig, 1971; pp 147 ff.
(39) Dorset, D. L.; Hanlon, J.; Karet, G. *Macromolecules* **1989**, *22*, 2169.
(40) Abrahamsson, S.; Dahlén, B.; Löfgren, H.; Pascher, I. *Progr. Chem. Fats Other Lipids* **1978**, *16*, 125.